Precipitation control and activation enhancement in boron-doped p + -BaSi2 films grown by molecular beam epitaxy

M. Ajmal Khan, K. Nakamura, W. Du, K. Toko, N. Usami, and T. Suemasu

---

Articles you may be interested in

Improved photoresponsivity of semiconducting BaSi2 epitaxial films grown on a tunnel junction for thin-film solar cells
Appl. Phys. Lett. **100**, 152114 (2012); 10.1063/1.3703585

Minority-carrier diffusion length, minority-carrier lifetime, and photoresponsivity of -FeSi2 layers grown by molecular-beam epitaxy
J. Appl. Phys. **109**, 123502 (2011); 10.1063/1.3596565

Mn doping and p -type conductivity in zinc-blende GaMnN layers grown by molecular beam epitaxy
J. Vac. Sci. Technol. B **23**, 1294 (2005); 10.1116/1.1868699

Mg doping of GaN layers grown by plasma-assisted molecular-beam epitaxy
Appl. Phys. Lett. **76**, 718 (2000); 10.1063/1.125872

Two-dimensional arsenic precipitation in superlattice structures of alternately undoped and heavily Be-doped GaAs grown by low-temperature molecular beam epitaxy
Appl. Phys. Lett. **72**, 1984 (1998); 10.1063/1.121240

Precipitation control and activation enhancement in boron-doped p+-BaSi2 films grown by molecular beam epitaxy

M. Ajmal Khan,[1] K. Nakamura,[1] W. Du,[1] K. Toko,[1] N. Usami,[2,3] and T. Suemasu[1,3]

[1]*Institute of Applied Physics, University of Tsukuba, Tsukuba, Ibaraki 305-8573, Japan*
[2]*Graduate School of Engineering, Nagoya University, Chikusa-ku, Nagoya 464-8603, Japan*
[3]*Japan Science and Technology Agency, Core Research for Evolutionary Science and Technology, Tokyo 102-0075, Japan*

Precipitation free boron (B)-doped as-grown p+-BaSi2 layer is essential for the BaSi2 p-n junction solar cells. In this article, B-doped p-BaSi2 layers were grown by molecular beam epitaxy on Si(111) substrates, and the influence of substrate growth temperature (T_S) and B temperature (T_B) in the Knudsen cell crucible were investigated on the formation of B precipitates and the activation efficiency. The hole concentration, p, reached 1.0×10^{19} cm^{-3} at room temperature for $T_S = 600$ and $T_B = 1550$ °C. However, the activation rate of B was only 0.1%. Furthermore, the B precipitates were observed by transmission electron microscopy (TEM). When the T_S was raised to 650 °C and the T_B was decreased to 1350 °C, the p reached 6.8×10^{19} cm^{-3}, and the activation rate increased to more than 20%. No precipitation of B was also confirmed by TEM. © *2014 AIP Publishing LLC.*
[http://dx.doi.org/10.1063/1.4885553]

To decrease the levelized cost of solar electricity as well as emissions of greenhouse gases into the environment, it is required for solar cells to achieve high efficiency. More preferably, the solar cell materials are composed of earth abundant elements. Recently, thin-film solar cell materials, such as chalcopyrites and CdTe, have been attracting attention from the view point of their high optical absorption coefficient and cost-effective growth procedure.[1–4] A lot of studies have also been carried out on thin-film Si solar cells by utilizing an efficient light trapping system;[5–14] however, it is not easy to achieve efficiencies as high as Si bulk crystals. Thus, exploring different materials other than Si, Cu(In,Ga)Se2, and III-V compound semiconductors is also very important. Among such materials, we have focused much attention on semiconducting barium disilicide (BaSi2) for thin-film solar cell applications. Composed of earth-abundant Ba and Si, BaSi2 has a band gap of approximately 1.3 eV,[15,16] and a long minority carrier diffusion length, L, of approximately 10 μm,[17] and thereby a long minority-carrier lifetime (>10 μs).[18–20] One of the most important features of BaSi2 is that it has a large absorption coefficient, α, exceeding 3×10^4 cm^{-1} for photon energies greater than the band gap in spite of its indirect band gap nature.[16] The direct transition occurs approximately 0.1 eV above the band gap.[21,22] Large L and large α facilitate to collect the photogenerated carriers in BaSi2. We have achieved large photocurrent corresponding to the internal quantum efficiency exceeding 70% for the 400 nm-thick undoped n-BaSi2 layer grown on the Sb-doped n+-BaSi2/p+-Si tunnel junction.[23] Thus, the remaining step is the formation of a p-n junction. Since the top of valence band in BaSi2 is mostly composed of Si 3s and 3p orbitals,[21,22,24–26] impurity doping of group-III and group-V elements enables us to control the carrier type and conductivity of BaSi2 theoretically[27] and experimentally.[28–30] As a p-type dopant, B is considered a suitable candidate.[30] Very recently, we have controlled the hole concentration of B-doped BaSi2 in a wide range between 10^{17} and 10^{20} cm^{-3} at room

temperature (RT) by changing the temperature of the B Knudsen cell crucible. The built-in voltage of the p-n diode, thereby the open-circuit voltage, is limited by the difference in work function between the n- and p-type films. Thus, the heavily p-type doping is of essential importance. In the previous work, however, post annealing at 800 °C for 2 min was inevitable to realize an activation efficiency of 10%.[30] Most impurities, such as Al, Sb, and As, except B have large diffusion coefficients in the BaSi2 layers.[31–34] Thus, the enhancement of activation efficiency in low-temperature grown B-doped BaSi2 without post annealing is necessary to realize a sharp p-n junction. Furthermore, it was found that the B-doped BaSi2 layers contain precipitated B clusters due to low substrate temperature as well as heavily doping of elemental B. The precipitated B clusters could deteriorate the minority carrier properties of the film. In this article, we investigated the influence of substrate growth temperature and B temperature in the Knudsen cell crucible on the formation of B precipitates and the activation efficiency. By optimizing the above conditions, we achieved the hole concentration of 6.8×10^{19} cm^{-3} in the as-grown precipitation-free B-doped BaSi2 films, and the activation rate exceeded 20%.

An ion-pumped molecular beam epitaxy (MBE) system equipped with standard Knudsen cells for Ba and B sources and an electron-beam evaporation source for Si was used for the growth of B-doped BaSi2 films. Details of the growth procedures are provided previously.[28–30] Briefly, a 10-nm-thick BaSi2 epitaxial film was first grown by reactive deposition epitaxy on floating-zone n-Si(111) substrates ($\rho > 1000$ Ω·cm) at substrate temperature, T_S, of 510 °C, and then it was used as a template layer for BaSi2 overlayers. Then, Ba, Si, and B were co-evaporated on the BaSi2 template at $T_S = 600$ (sample A) or 650 °C (samples B and C) to form approximately 0.25–μm-thick a-axis-oriented B-doped BaSi2 epitaxial films by MBE. The temperature of B crucible, T_B, was varied as 1550, 1450, and 1350 °C, respectively, for samples A-C. The electrical properties were characterized at RT by Hall

measurements using the van der Pauw method. Depth profiles of B atoms in B-doped $BaSi_2$ films were characterized by secondary ion mass spectroscopy (SIMS) using O^2 ions. The crystalline qualities of the samples were characterized by out-of-plane θ–2θ x-ray diffraction (XRD) and in-plane ϕ–$2\theta_\chi$ XRD using Cu-$K\alpha$ x-ray (wavelength 1.5418 Å). In the ϕ–$2\theta_\chi$ XRD measurement, the scattering vector was set along the in-plane $Si[\bar{1}10]$ direction. In order to investigate the domain boundaries of $BaSi_2$ and B precipitates, plan-view transmission electron microscopy (TEM) samples prepared by mechanical polishing and ion milling were observed using TOPCON EM-002B operated at 120 kV.

Figure 1(a) shows the θ–2θ XRD patterns of samples A-C. Diffraction peaks of (100)-oriented $BaSi_2$ were confirmed. Reflection high-energy electron diffraction exhibited streaky patterns for all the samples, meaning that B-doped $BaSi_2$ films were epitaxially grown. However, we see the peak at around $2\theta = 36°$ corresponding to the rhombohedral B(110) plane in samples A and B. This result suggests that the $BaSi_2$ films contain B precipitates in those samples. On the other hand, the diffraction peak of B was not observed in the θ–2θ XRD patterns for sample C. In order to enhance the detection sensitivity of grown layers in sample C, we performed the in-plane ϕ–$2\theta_\chi$ XRD measurement on sample C as shown in Fig. 1(c). Although we see intense diffraction peaks of $BaSi_2$(020) and (040) planes, diffractions due to B precipitates are difficult to observe.

Figures 2(a)–2(c) show the plan-view TEM images. The incident beam direction was almost parallel to the $BaSi_2$[100] zone axis, but was slightly tilted for the domain boundaries to be seen clearly. Because domain boundaries are parallel to the surface normal, their contrast vanishes in the exact [100] zone axis. As shown in Figs. 2(a) and 2(b), we see a lot of B precipitates in samples A and B. The size of B precipitates is approximately 5 and 3 nm in diameters, respectively. a-axis-oriented $BaSi_2$ film consists of three epitaxial domains rotating 120° around the surface normal with each other, and the domain boundaries are quite sharp in undoped $BaSi_2$ films.[17] In contrast, the domain boundaries of

FIG. 1. (a) θ-2θ XRD patterns (out-of-plane) of samples A-C, and (b) ϕ-$2\theta_\chi$ XRD pattern (in-plane) of sample C. The asterisk shows the diffraction from the Si substrate.
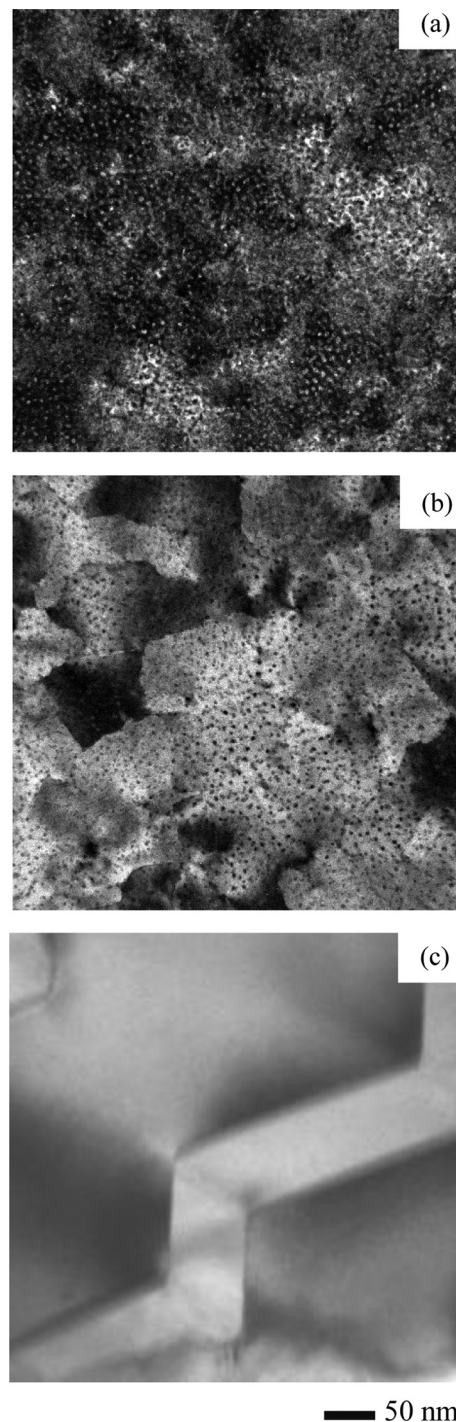
FIG. 2. (a)-(c) Bright-field plan-view TEM images along the [100] azimuth of $BaSi_2$ for samples A-C, respectively.

the B-doped BaSi$_2$ film in sample A are not clearly observed in Fig. 2(a). We see the same tendency in sample B, and the domain boundaries are roundish in Fig. 2(b). We should note here, in Fig. 2(c), that we cannot observe B precipitates in sample C. In addition, the domain boundaries are quite sharp like those in undoped BaSi$_2$ films. It is reasonable to think that the decrease of T_B resulted in the decrease of N_B, and additional higher T_S increases the solubility limit of B in BaSi$_2$ and enables us to form the precipitation-free B-doped BaSi$_2$ film in sample C.

Next, we discuss the electrical properties of the B-doped BaSi$_2$ films. The electrical properties are summarized in Table I. The hole concentration, p, in the B-doped BaSi$_2$ gradually increased from 1.0×10^{19} cm^{-3} in sample A to 6.8×10^{19} cm^{-3} in sample C at RT. The acceptor level, E_A, calculated using Eq. (1) was almost the same as approximately 23 meV as shown in Fig. 3(a)

$$p \propto \exp\left(-\frac{E_A}{2k_B T}\right). \tag{1}$$

Here, k_B is the Boltzmann's constant, and T the absolute temperature.

Figure 3(b) shows the T_B dependence of N_B. The inset shows one example of the SIMS depth profiles of B atoms (sample A). The N_B values in the SIMS profiles were corrected using reference samples, where controlled number of B atoms was doped in the BaSi$_2$ films by ion implantations. The obtained B concentrations are explained relatively well by the difference in vapor pressure of B. From the macroscopic viewpoint, the doped B atoms were relatively uniformly distributed within the layers. The average N_B decreased from 1×10^{22} to 2×10^{21} and 3×10^{20} cm^{-3}, in samples A-C, respectively. The activation efficiency of B atoms can thus be estimated, that is, $p/N_B = 0.1$ (sample A), 3 (sample B), and $>20\%$ (sample C). This value of 20% is the highest ever achieved for p^+-BaSi$_2$. Higher T_S than 650 °C might enhance the activation efficiency of B and therefore result in a higher p. However, the low-T_S formation of B-doped BaSi$_2$ layers is inevitable when we grow a BaSi$_2$ p-n diode structure since the diffusion coefficients of impurities atoms, especially n-type dopants, such as Sb and P, are large.[33,34] According to the previous work,[30] when the T_S was lowered down to 600 °C for $T_B = 1350$ °C, it was difficult to obtain reliable p values due to difficulties in forming ohmic contacts on the surface.[30] The effective density of states of valence band is approximately 2.0×10^{19} cm^{-3} from the effective mass tensors of hole in BaSi$_2$.[21] Discussed in this way, it can safely be stated that the obtained p value of 6.8×10^{19} cm^{-3} is large enough for as-grown

TABLE I. Preparation of samples A-C: Growth temperature (T_S), temperature of B (T_B), measured B concentration (N_B), measured hole concentration (p), electrical resistivity (ρ), and activation efficiency of B atoms (p/N_B) are shown.

Sample	T_S (°C)	T_B (°C)	N_B (cm^{-3})	p (cm^{-3})	ρ ($\Omega\cdot$cm)	p/N_B (%)
A	600	1550	1×10^{22}	1.0×10^{19}	0.099	0.1
B	650	1450	2×10^{21}	6.5×10^{19}	0.12	3
C	650	1350	3×10^{20}	6.8×10^{19}	0.092	>20
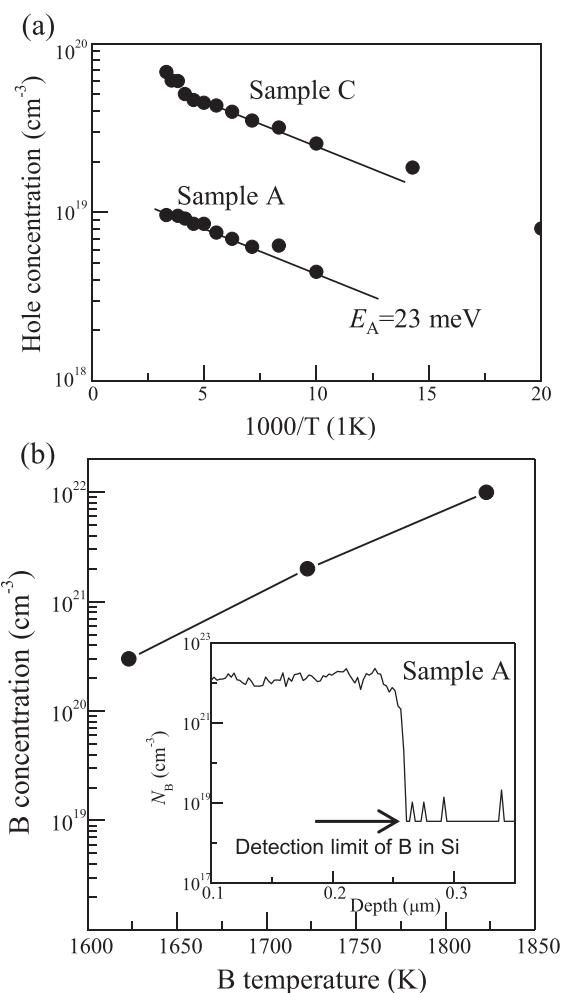
FIG. 3. (a) Temperature dependences of hole concentration for samples A and C. (b) T_B dependence of N_B. The inset shows the SIMS depth profile of B in sample A.

precipitation-free B-doped BaSi$_2$ films formed at low T_S. Regarding the remaining 80% B atoms, we speculate that there is the possibility that B atoms occupy the interstitial sites of the unite cell of BaSi$_2$ because BaSi$_2$ has a relatively low-dense structure. In Ref. 35, it is described that interstitial compounds of magnetic elements (Mn, Fe, Co, and Ni) and BaSi$_2$ are energetically possible. Since B is much smaller than these magnetic elements, occupation of B atoms in the interstitial sites is probable. A first-principle calculation may help us to discuss further on this matter.

In conclusion, we have achieved precipitation-free B-doped heavily p-type doping in BaSi$_2$ by MBE. By decreasing the T_B from 1550 to 1350 °C, thereby the average N_B from 1×10^{22} to 3×10^{20} cm^{-3} and by increasing the T_S from 600 to 650 °C, the precipitation-free B-doped BaSi$_2$ films were achieved. We have realized the hole concentration of 6.8×10^{19} cm^{-3} and the activation rate exceeded 20% at RT without post annealing.

[1] A. Romeo, A. Terheggen, D. Abou-Ras, D. L. Batzner, F. J. Haug, M. Kalin, D. Rudmann, and A. N. Tiwari, Prog. Photovoltaics **12**, 93 (2004).

[2] I. Repins, M. A. Contreras, B. Egaas, C. DeHart, J. Scharf, C. L. Perkins, B. To, and R. Noufi, Prog. Photovoltaics **16**, 235 (2008).

[3] P. Jackson, D. Hariskos, E. Lotter, S. Paetel, R. Wuerz, R. Menner, W. Wischmann, and M. Powalla, Prog. Photovoltaics **19**, 894 (2011).

[4] H. Katagiri, K. Jimbo, W. S. Maw, K. Oishi, M. Yamazaki, H. Araki, and A. Takeuchi, Thin Solid Films **517**, 2455 (2009).

[5] R. G. Gordon, J. Proscia, F. B. Ellis, Jr., and A. E. Delahoy, Sol. Energy Mater. **18**, 263 (1989).

[6] P. Campbell, Sol. Energy Mater. **21**, 165 (1990).

[7] J. Meier, S. Dubail, R. Platz, P. Torres, U. Kroll, J. A. A. Selvan, N. P. Vaucher, Ch. Hof, D. Fischer, H. Keppner, R. Flückiger, A. Shah, V. Shklover, and K.-D. Ufert, Sol. Energy Mater. Sol. Cells **49**, 35 (1997).

[8] O. Vetterl, F. Finger, R. Carius, P. Hapke, L. Houben, O. Kluth, A. Lambertz, A. Mück, B. Rech, and H. Wagner, Sol. Energy Mater. Sol. Cells **62**, 97 (2000).

[9] A. Poruba, A. Fejfar, Z. Remes, J. Springer, M. Vanecek, and J. Kocka, J. Appl. Phys. **88**, 148 (2000).

[10] J. Müller, B. Rech, J. Springer, and M. Vanecek, Sol. Energy **77**, 917 (2004).

[11] M. Berginski, J. Hüpkes, M. Schulte, G. Schöpe, H. Stiebig, and B. Rech, J. Appl. Phys. **101**, 074903 (2007).

[12] D. Zhou and R. Biswas, J. Appl. Phys. **103**, 093102 (2008).

[13] A. Hongsingthong, T. Krajangsang, I. A. Yunaz, S. Miyajima, and M. Konagai, Appl. Phys. Express **3**, 051102 (2010).

[14] H. Sai, Y. Kanamori, and M. Kondo, Appl. Phys. Lett. **98**, 113502 (2011).

[15] K. Morita, Y. Inomata, and T. Suemasu, Thin Solid Films **508**, 363 (2006).

[16] K. Toh, T. Saito, and T. Suemasu, Jpn. J. Appl. Phys., Part 1 **50**, 068001 (2011).

[17] M. Baba, K. Toh, K. Toko, N. Saito, N. Yoshizawa, K. Jiptner, T. Sekiguchi, K. O. Hara, N. Usami, and T. Suemasu, J. Cryst. Growth **348**, 75 (2012).

[18] K. O. Hara, N. Usami, K. Toh, M. Baba, K. Toko, and T. Suemasu, J. Appl. Phys. **112**, 083108 (2012).

[19] K. O. Hara, N. Usami, K. Nakamura, R. Takabe, M. Baba, K. Toko, and T. Suemasu, Appl. Phys. Express **6**, 112302 (2013).

[20] R. Takabe, K. O. Hara, M. Baba, W. Du, N. Shimada, K. Toko, N. Usami, and T. Suemasu, J. Appl. Phys. **115**, 193510 (2014).

[21] D. B. Migas, V. L. Shaposhnikov, and V. E. Borisenko, Phys. Status Solidi B **244**, 2611 (2007).

[22] M. Kumar, N. Umezawa, and M. Imai, J. Appl. Phys. **115**, 203718 (2014).

[23] W. Du, M. Suzuno, M. Ajma Khan, K. Toh, M. Baba, K. Nakamura, K. Toko, N. Usami, and T. Suemasu, Appl. Phys. Lett. **100**, 152114 (2012).

[24] Y. Imai, A. Watanabe, and M. Mukaida, J. Alloys Compd. **358**, 257 (2003).

[25] S. Kishino, T. Imai, T. Iida, Y. Nakaishi, M. Shinada, Y. Takanashi, and N. Hamada, J. Alloys Compd. **428**, 22 (2007).

[26] M. Baba, K. Ito, W. Du, T. Sanai, K. Okamoto, K. Toko, S. Ueda, Y. Imai, A. Kimura, and T. Suemasu, J. Appl. Phys. **114**, 123702 (2013).

[27] Y. Imai and A. Watanabe, Intermetallics **15**, 1291 (2007).

[28] M. Kobayashi, Y. Matsumoto, Y. Ichikawa, D. Tsukada, and T. Suemasu, Appl. Phys. Express **1**, 051403 (2008).

[29] M. Ajmal Khan, T. Saito, K. Nakamura, M. Baba, W. Du, K. Toko, and T. Suemasu, Thin Solid Films **522**, 95 (2012).

[30] M. Ajmal Khan, K. O. Hara, W. Du, M. Baba, K. Nakamura, M. Suzuno, K. Toko, N. Usami, and T. Suemasu, Appl. Phys. Lett. **102**, 112107 (2013).

[31] K. Nakamura, M. Baba, K. M. Ajmal, W. Du, M. Sasase, K. O. Hara, N. Usami, K. Toko, and T. Suemasu, J. Appl. Phys. **113**, 053511 (2013).

[32] K. Nakamura, K. Toh, M. Baba, K. M. Ajmal, W. Du, K. Toko, and T. Suemasu, J. Cryst. Growth **378**, 189 (2013).

[33] K. O. Hara, Y. Hoshi, N. Usami, Y. Shiraki, K. Nakamura, K. Toko, and T. Suemasu, Thin Solid Films **557**, 90 (2014).

[34] N. Zhang, K. Nakamura, M. Baba, K. Toko, and T. Suemasu, Jpn. J. Appl. Phys., Part 1 **53**, 04ER02 (2014).

[35] Y. Imai, M. Sohama, and T. Suemasu, J. Magn. Magn. Mater. **344**, 25 (2013).